Electronic Supplementary Material (ESI) for Inorganic Chemistry Frontiers.

Solvent-dependent Valence-Tautomerism and Polarization Switching in a Heterodinuclear Complex

Wenwei Zheng[a], Xiaopeng Zhang[a], Qirui Shui[a], Tatsuki Fukuyama[a], Wen-huang Xu[a], Yu-bo Huang[a], Tianchi Ji[a], Ziqi Zhou[a], Mikoto Uematsu[a], Sheng-Qun Su[a], Shinji Kanegawa[a], Shu-Qi Wu*, and Osamu Sato*

a. Institute for Material Chemistry and Engineering, Kyushu University, 744 Motooka, Nishi-ku, Fukuoka, 819-0395, Japan

Synthesis and Methods

Materials

All reagents were commercially purchased by Tokyo Chemical Industry Co., Ltd., FUJIFILM Wako, Pure Chemical Corporation, and Sigma-Aldrich Company, and directly used without further purification. 5,5,7,12,12,14-hexamethyl-1,4,8,11-tetraazacyclotetradecane (*Rac*-cth) and its enantiopure chiral ligand (*SS*-cth) were synthesized as previously reported method.[1] All reactions were conducted under N_2 gas.

Synthesis of $[Co(AcO)(SS\text{-}cth)]PF_6$

$Co(AcO)_2{\cdot}4H_2O$ (750 mg, 3.0 mmol) and *SS*-cth (850 mg, 3.0 mmol) were added into ethanol (10 ml). The solution was stirred and heated to 60 °C. After that, NH_4PF_6 (540 mg, 3.3 mmol) was added to this solution and pink solid of $[Co(AcO)(SS\text{-}cth)]PF_6$ was gradually precipitated. The solution was cooled down by ice-bath, then the participation was filtered and washed with cold ethanol followed by Et_2O. $[Co(AcO)(SS\text{-}cth)]PF_6$ was obtained of about 0.96 g, yield: 76.1%.

Synthesis of enantiopure $[CrCl_2(SS\text{-}cth)]Cl$

$[CrCl_2(SS\text{-}cth)]Cl$ was synthesized in the same method as reported literature for $[CrCl_2(Rac\text{-}cth)]Cl$ using optically pure *SS*-cth as a starting material to afford a greenish-blue solid product (yield = 68.0%).[2]

Synthesis of enantiopure $[Zn(Aco)(SS\text{-}cth)]PF_6$

The $[Zn(AcO)(SS\text{-}cth)]PF_6$ was synthesized in the same method with $[Co(Ac)(SS\text{-}cth)]PF_6$ using $Zn(AcO)_2$ (550 mg, 3 mmol) as starting material to afford a white solid product (yield = 70%).

Synthesis of enantiopure $[Ni(Aco)(SS\text{-}cth)]PF_6$

The $[Ni(AcO)(SS\text{-}cth)]PF_6$ was synthesized in the same method with $[Co(Ac)(SS\text{-}cth)]PF_6$ using $Ni(AcO)_2{\cdot}4H_2O$ (746 mg, 3 mmol) as starting material to afford a blue solid product (yield = 72%).

Synthesis of precursor [Cr(*SS*-cth)(μ-dhbq)]PF_6

A mixture of 3,5-dihydroxy-1,4- benzoquinone (H_2dhbq;140 mg, 1 mmol) and triethylamine (202 mg, 2.0 mmol) in methanol (50 ml) was stirred under an inert atmosphere. Then, solid [$CrCl_2$(*SS*-cth)]Cl (443 mg, 1 mmol) was added to the solution, and heated up to 60 ℃ for one hour. An aqueous of $LiPF_6$ (300 mg, 2 mmol) was added into the dark-red solution. Slow evaporation led to the dark red participate [Cr(*SS*-cth)(μ-dhbq)]PF_6. The precipitation was filtered and washed by H_2O (yield = 80%).

Synthesis of [Co(*SS*-cth)(μ-dhbq)Cr(*SS*-cth)]$(PF_6)_3$

One-pot synthetic method: The [CrCo] with enantiopure ligands was synthesized as the previously reported method. Directly mix mononuclear [Co(AcO)(*SS*-cth)]PF_6 (547.5 mg, 1 mmol) and [$CrCl_2$(*SS*-cth)]Cl (443 mg 1 mmol) in the dhbq solution to afford the crude product of [Co(*SS*-cth)(μ-dhbq)Cr(*SS*-cth)]$(PF_6)_3$.

Stepwise synthetic method: The mixture of [Co(AcO)(*SS*-cth)]PF_6 (547.5 mg, 1 mmol) and [Cr(*SS*-cth)(μ-dhbq)]PF_6 (619.5 mg, 1 mmol) was added to Methanol (50 ml) under N_2 gas. The reaction solution was stirred at room temperature for 1 hour and then an aqueous of KPF_6 (227 mg, 1.5 mmol) was added to the methanol solution. Keep stirring the mixture overnight to precipitate purple-red [Co(*SS*-cth)(μ-dhbq)Cr(*SS*-cth)]$(PF_6)_3$. The precipitation was filtered and washed with water, and then completely dry under reduced pressure. The crude product was crystallized in the mixed solution of Methanol/H_2O with drops of acetonitrile to afford a red stick-shaped crystal (yield = 239 mg, 83%).

Synthesis of [Ni(*SS*-cth)(μ-dhbq)Cr(*SS*-cth)]$(PF_6)_3$

One-pot synthetic method: The [CrNi] with enantiopure ligands was synthesized as the previously reported method.[3] Directly mix mononuclear [Ni(AcO)(*SS*-cth)]PF_6 (546.5 mg, 1 mmol) and [$CrCl_2$(*SS*-cth)]Cl (443 mg 1 mmol) in the dhbq solution to afford the crude product of [Ni(*SS*-cth)(μ-dhbq)Cr(*SS*-cth)]$(PF_6)_3$.

Stepwise synthetic method: The mixture of [Ni(AcO)(*SS*-cth)]PF_6 (546.5 mg, 1 mmol) and [Cr(*SS*-cth)(μ-dhbq)]PF_6 (619.5 mg, 1 mmol) was added to Methanol (50 ml) under N_2 gas. The reaction solution was stirred at room temperature for 1 hour and then an aqueous of KPF_6 (227 mg, 1.5 mmol) was added to the methanol solution. Keep stirring the mixture overnight to precipitate brown product [Ni(*SS*-cth)(μ-dhbq)Cr(*SS*-cth)]$(PF_6)_3$.

Synthesis of [Zn(*SS*-cth)(μ-dhbq)Cr(*SS*-cth)]$(PF_6)_3$

One-pot synthetic method: The [CrNi] with enantiopure ligands was synthesized as the previously reported method. Directly mix mononuclear [Zn(AcO)(*SS*-cth)]PF_6 (553.5 mg, 1 mmol) and [$CrCl_2$(*SS*-cth)]Cl (443 mg 1 mmol) in the dhbq solution to afford the crude product of [Zn(*SS*-cth)(μ-dhbq)Cr(*SS*-cth)]$(PF_6)_3$.

Stepwise synthetic method: The mixture of [Zn(AcO)(*SS*-cth)]PF_6 (553.5 mg, 1 mmol) and [Cr(*SS*-cth)(μ-dhbq)]PF_6 (619.5 mg, 1 mmol) was added to Methanol (50 ml) under N_2 gas. The reaction solution was stirred at room temperature for 1 hour and then an aqueous of KPF_6 (227 mg, 1.5 mmol) was added to the methanol solution. Keep stirring the mixture overnight to precipitate red product [Zn(*SS*-cth)(μ-dhbq)Cr(*SS*-cth)]$(PF_6)_3$.

X-ray diffraction measurement and crystal structural determinations

Diffraction data were collected at 100, and 200 K for **1·sol** under a nitrogen gas stream. Compound **1** was *in situ* obtained by heating the crystal at 375 K for 30 mins to remove the solvents. The diffraction data were collected for **1** at 100, 150, and 375 K. The measurement was performed on a Rigaku XtaLab Synergy-R/DW diffractometer equipped with a HyPix-6000 area detector and multi-layer mirror monochromated Mo-Kα radiation of λ= 0.71073 Å. The structures were solved by a direct method and refined via full-matrix least-squares on F^2 using the SHELX program[4] implemented in the OLEX2 program[5] with anisotropic thermal parameters for all non-hydrogen atoms. The hydrogen atoms were geometrically added and refined by the riding model.

Magnetic susceptibility measurement

Magnetic measurement was performed on a quantum design SQUID magnetometer (MPMS-5S). Polycrystalline samples (*ca.* ~ 10 mg) were loaded into the gelatin capsule and held by a plastic straw, which was fixed on a sample rod. The whole measurement was carried out under H = 2000 Oe with a sweeping rate of 2 k min^{-1}.

Pyroelectric measurement

Pyroelectric measurements were conducted using a continuous temperature ramping technique with a Keithley 6517B electrometer and a Quantum Design MPMS-XL chamber for precise temperature control. The single-crystal sample was carefully sandwiched between silver paste (with an area of 0.0598 mm^2) on its (010) and (0-10) surfaces to ascertain the direction of the pyroelectric current. The measurement temperature range was maintained between 30 and 250 K, with a helium gas flow ensuring thermal stability. The measurements were performed at a temperature sweep rate of 10 K min^{-1}.

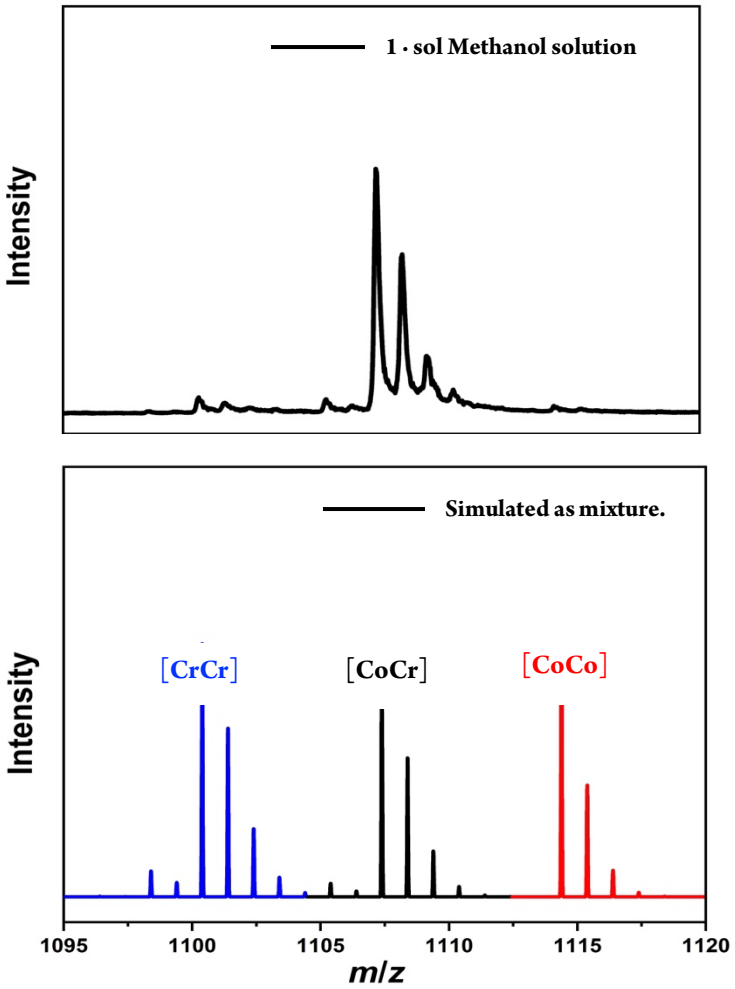

Figure S1. Electrospray Ionization Mass Spectrometry (ESI-MS) spectrum of **1·sol** in Methanol solution. (a) The spectrum exhibits the molecular peak of $[1(PF_6)_2]^+$ (m/z = 1107.3). It is noted that almost all the peaks are contributed by the $[1(PF_6)_2]^+$, even though there are still minor peaks from $[(CoCo)(PF_6)_2]^+$, it could be considered that partial dissociative mononuclear Co was oxidized by oxygen dissolved in Methanol to form dinuclear Co complex. However, it supports the target complex is basically stable and pure enough under solution condition. Besides, the purity of **1·sol** could also be confirmed by PXRD, elemental analysis, and crystal structure. (b) Simulation of the equimolar mixture for $[(CoCo)(PF_6)_2]^+$/$[(CoCr)(PF_6)_2]^+$/$[(CrCr)(PF_6)_2]^+$.

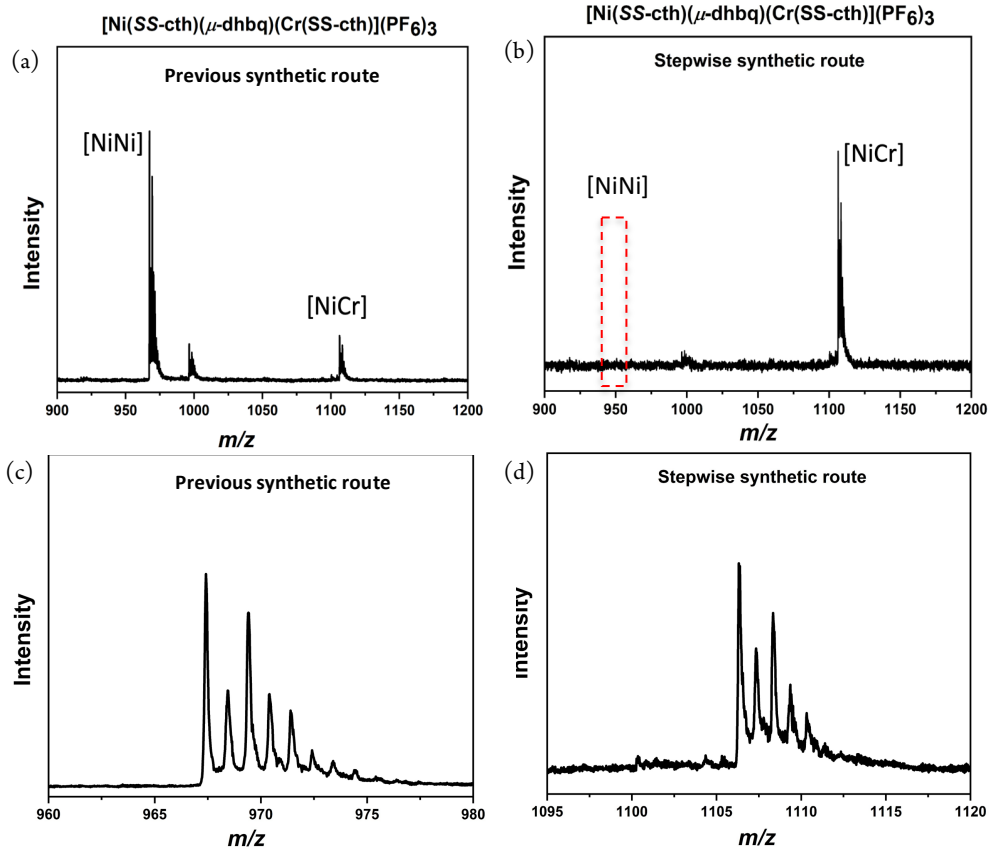

Figure S2. (a) The ESI-MS of $[(NiCr)(PF_6)_2]^+$ obtained by one-pot synthetic route. The result revealed that the predominant peak was contamination of $[(NiNi)(PF_6)]^+$ (m/z = 967.4). The desired complex of $[(NiCr)(PF_6)_2]^+$ (m/z = 1106.4) was found to occupy a minor proportion within the solution. This significant impurity poses a serious obstacle to subsequent purification processes. (b) In contrast, the step-wise synthetic route exhibited a mass spectrum characterized by unambiguous peaks from $[(NiCr)(PF_6)_2]^+$ (m/z = 1106.3) with the absence of $[(NiNi)(PF_6)]^+$ (m/z = 967.4). This observation validates our novel synthetic strategy is effective to avoid the generation of undesired side products. (c) The mass spectrum of $[(NiNi)(PF_6)]^+$ (m/z = 967.4). (d) The ESI-MS of $[(NiCr)(PF_6)_2]^+$ (m/z = 1106.3).

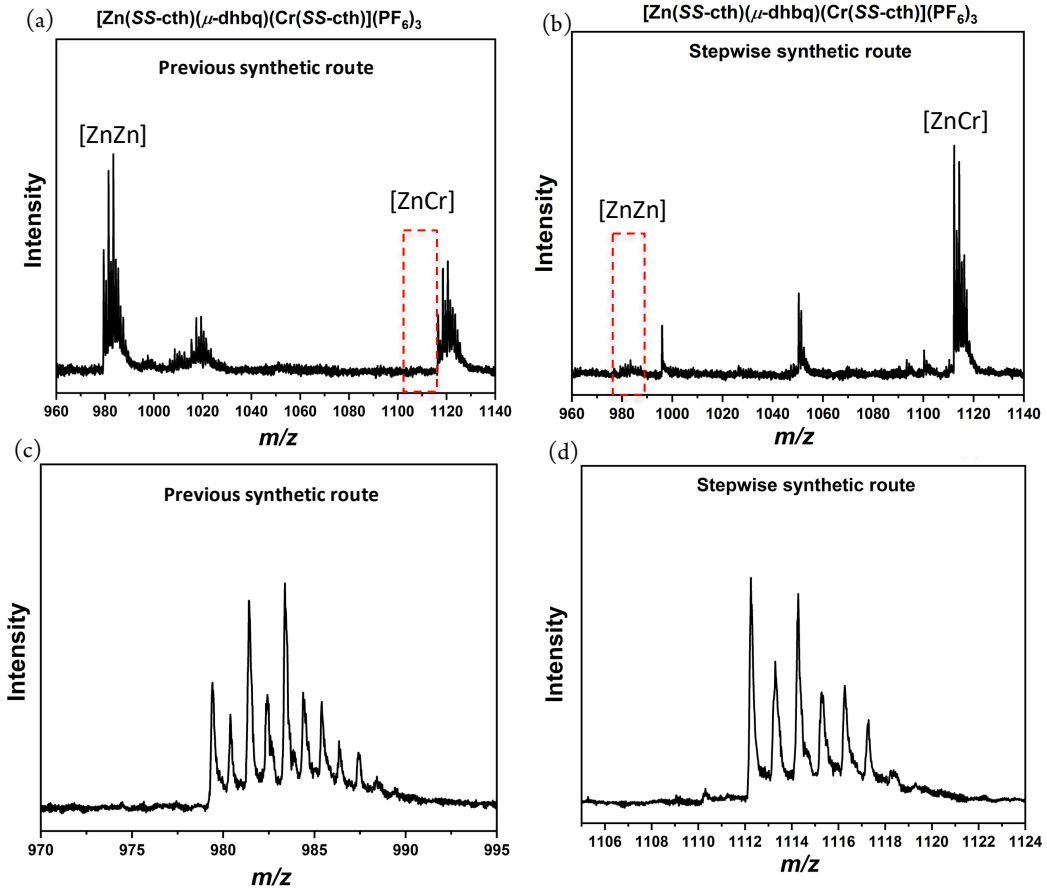

Figure S3 (a) It's noted that the ESI-MS of $[(ZnCr)(PF_6)_2]^+$ obtained by one-pot method revealed the peaks from $[(ZnZn)(PF_6)]^+$ (m/z = 981.4) instead of $[(ZnCr)(PF_6)_2]^+$. This discrepancy is probably owing to the faster reaction rate of mononuclear Zn compared with inert Cr. (b) On the other hand, employing a stepwise synthetic route resulted in a set of the peaks originated from $[(ZnCr)(PF_6)_2]^+$ (m/z = 1112.2). This finding confirms the stability of complex in the solution without signs of decomposition. Besides, the observed results align with the simulated one. Collectively, the analysis of these complexes, including reference and [CrCo] evident that utilizing the inert Cr to coordinate with one side of dhbq is reasonable and favorable to reduce the mixtures in heteronuclear complexes. (c) The mass spectrum of $[(ZnZn)(PF_6)]^+$ (m/z = 981.4). (d) The mass spectrum of $[(ZnCr)(PF_6)_2]^+$ (m/z = 1112.2).

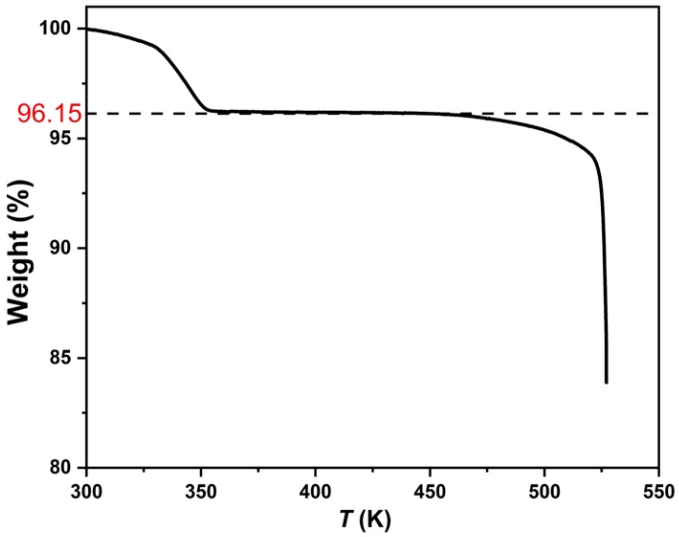

Figure S4. Thermal gravimetric analysis (TGA) was performed on compound 1·sol. The results revealed that complex 1·sol underwent desolvation with a weight loss of approximately 3.85% at a certain temperature. This almost corresponds to the loss of two lattice water molecules and half a methanol molecule. Upon further heating, the desolvated compound remained stable until approximately 460 K. The TGA results also suggested the solvents in the crystal lattice can be easily removed above 350 K.

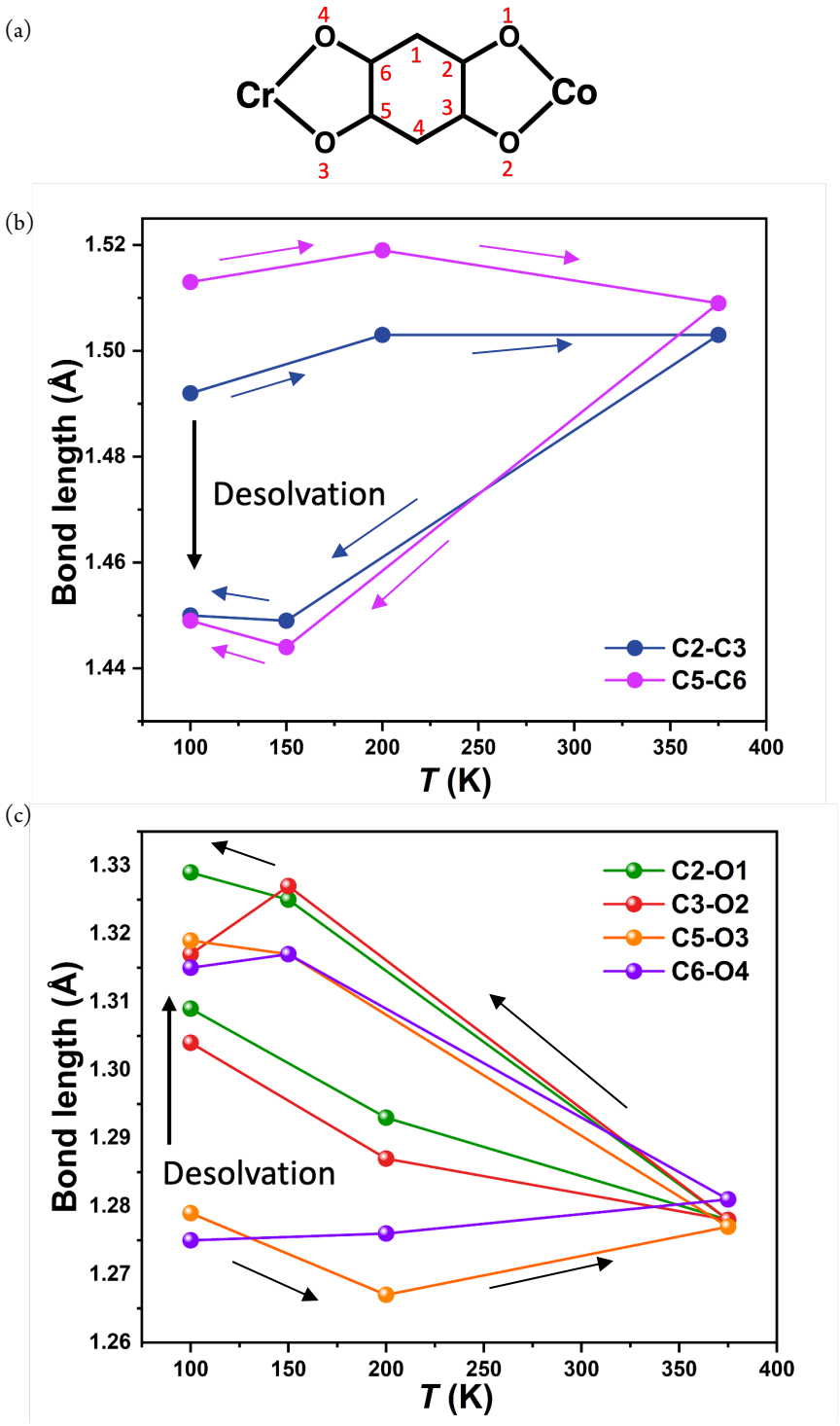

Figure S5. (a) Schematic illustration of specific carbon and oxygen from bridging ligand. (b) Temperature-dependent bond length of specific carbon-carbon before and after desolvation. (c) Temperature-dependent bond length of specific carbon-oxygen before and after desolvation.

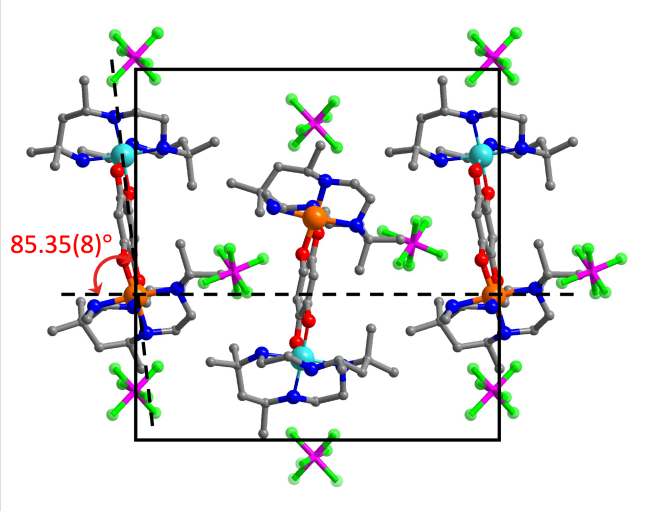

Figure S6. Crystal structure of compound **1** in 100 K. Compared with the crystal structure of compound 1 at 375 K, projection angle along crystallographic *b*-axis varies slightly.

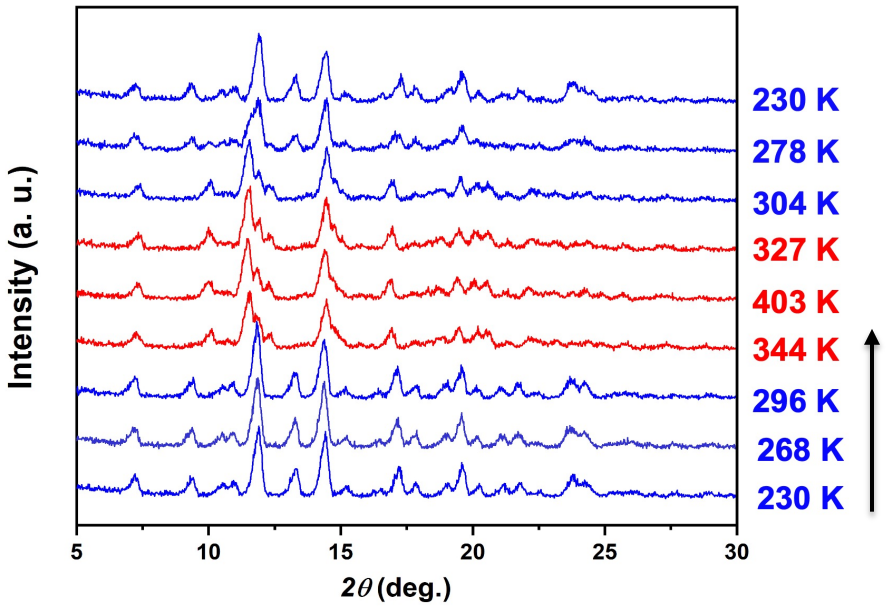

Figure S7. Thermally treated compound **1** was exposed to Methanol/H_2O and subsequently was performed on the PXRD with cycle of 230-400-230 K. The diffraction patterns at 230 K matched well with that of the pristine compound **1·sol.** Moreover, the variable tendency under heating and cooling mode agreed well with the temperature-dependent patterns in initial complex. This observation further confirmed the reversibility of single-crystal-to-single-crystal transformation.

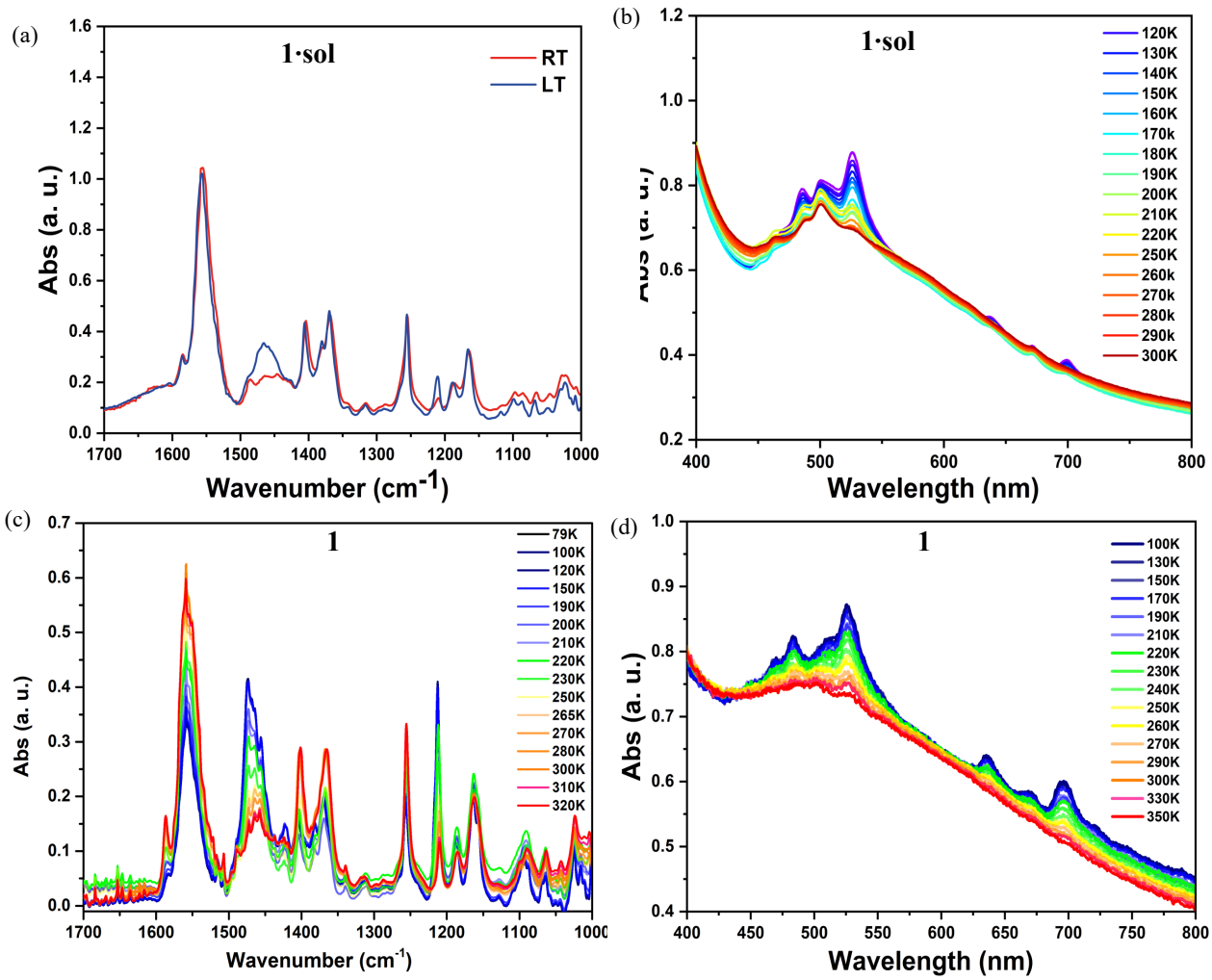

Figure S8. (a) Compound **1·sol** was pressed into KBr pellet and measured at room temperature and low temperature (the sample was cooled down by direct immersion in the liquid nitrogen). It is noted that the band at approximately 1470 cm^{-1} become intense, which could be assigned to the $dhsq^{3-}$. Accordingly, the band at around 1520 cm^{-1} assigned to the $dhbq^{2-}$ become weaker. This variation evidence that partial electron transfer between Co and dhbq ligand on **1·sol**. (b) Ground compound **1·sol** was uniformly attached the surface of tape and sealed with another tape. Temperature-dependent UV-vis was performed. (c) Ground sample compound **1·sol** was adhered to the surface of CaF_2 After the treatment of desolvation by heating the sample at 400 K for 30 min and transfer it to cryostat with a vacuum condition. Temperature-dependent IR spectrum of **1** was performed from 79 K to 320 K. (d) Temperature-dependent UV-vis spectrum of compound **1** from 100 K to 350 K the same treatment of sample with IR measurement.

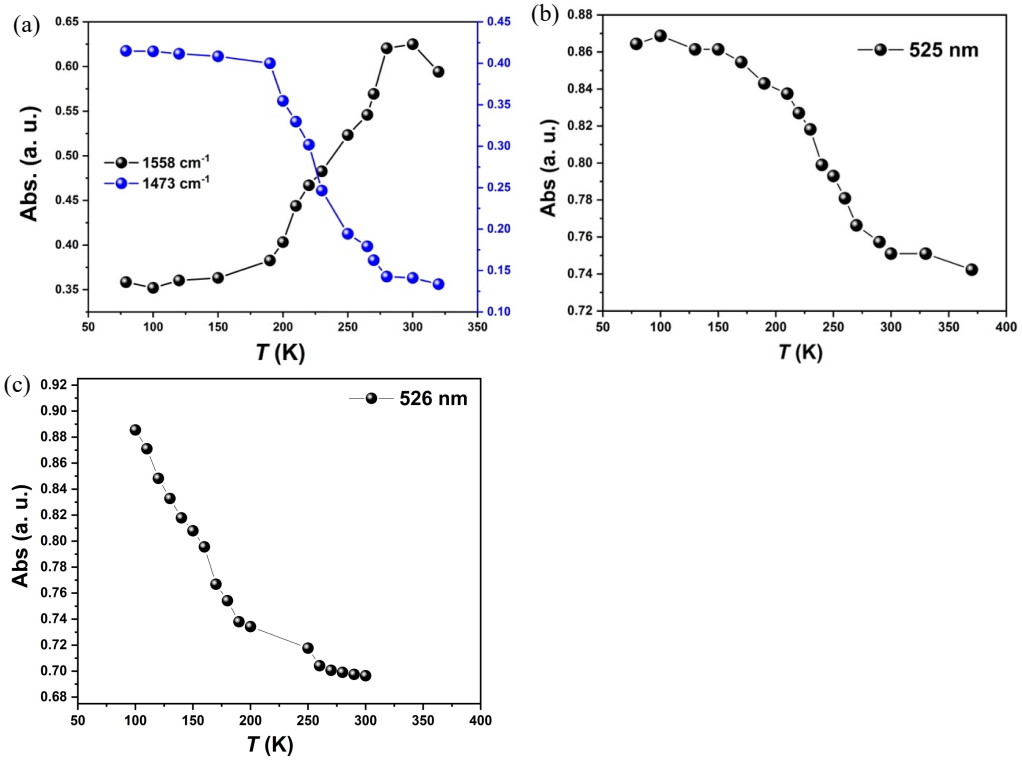

Figure S9. (a) The intensity of temperature-dependent IR absorption band in 1470 and 1558 cm^{-1} on compound **1**, corresponding to a transition from $dhbq^{2-}$ to $dhbq^{3-}$ as the temperature increase. The variation tendency of the band intensity was consistent with magnetization transition of compound **1** at the same temperature range. This observation supports the solvents of sample has been successfully removed and occurrence of electron transfer. (b) The intensity of temperature-dependent UV-vis absorption band in 525 nm on compound **1**. Similar variation to the temperature-dependent IR measurement of **1** at approximately 1473 cm^{-1}. (c) The intensity changes of variable-temperature UV-vis of **1·sol** on 526 nm. Different from the desolvated sample, the intensity of absorption band at 526 nm appears continuous changes from 100 K and end at around 250 K. As the variation of **1·sol** on magnetization, it confirms the origin of magnetic transition attribute to the electron transfer between Co^{2+} and $dhbq^{2-}$.

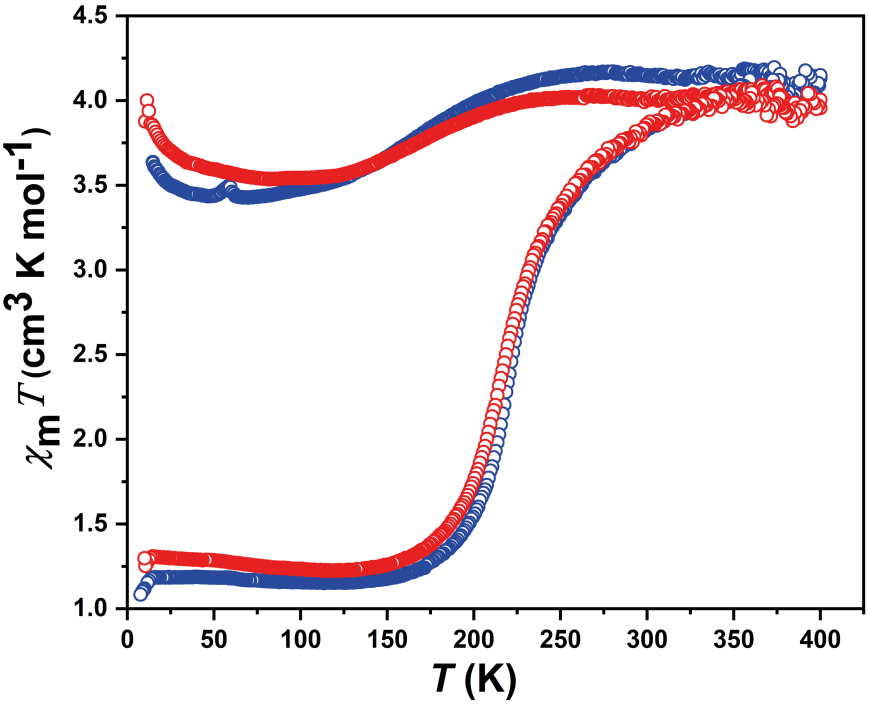

Figure S10. The blue circle is the magnetic susceptibility of refreshing **1·sol.** After a complete cycle of 10 – 400 – 10 K, the sample was taken out from the SQUID chamber and was placed above the mixture of Methanol/H_2O overnight. The reabsorbed sample was performed on the magnetization again to confirm the reversibility of solvent dependent magnetic property shown in red circle.

Table S1. Elemental analysis

	H%	C%	N%
1·sol (orginal one)	6.25	35.49	8.75
1·sol (reabsorbed)	6.22	35.27	8.47
Calculated result of **1.sol**	6.16	35.16	8.52

NiCr (previous method, reduced pressure vacuum)	6.60	40.63	9.76
NiCr (stepwise route, reduced pressure vacuum)	6.07	36.76	8.92
Calculated result of NiCr	5.91	36.39	8.94
ZnCr(previous method, reduced pressure vaccum)	6.75	39.59	9.88
ZnCr (stepwise route, reduced pressure vacuum)	6.03	36.50	8.92
Calculated result of ZnCr	5.88	36.22	8.90

Figure S11. The pyroelectric measurement was carried out as a previously reported method.[6-8] The single crystal for pyroelectric measurement (Left). The index of crystal (Right). To ensure the pyroelectric current could be detected by our electrometer, the area of plane (010) should be at least 0.04 mm^2.

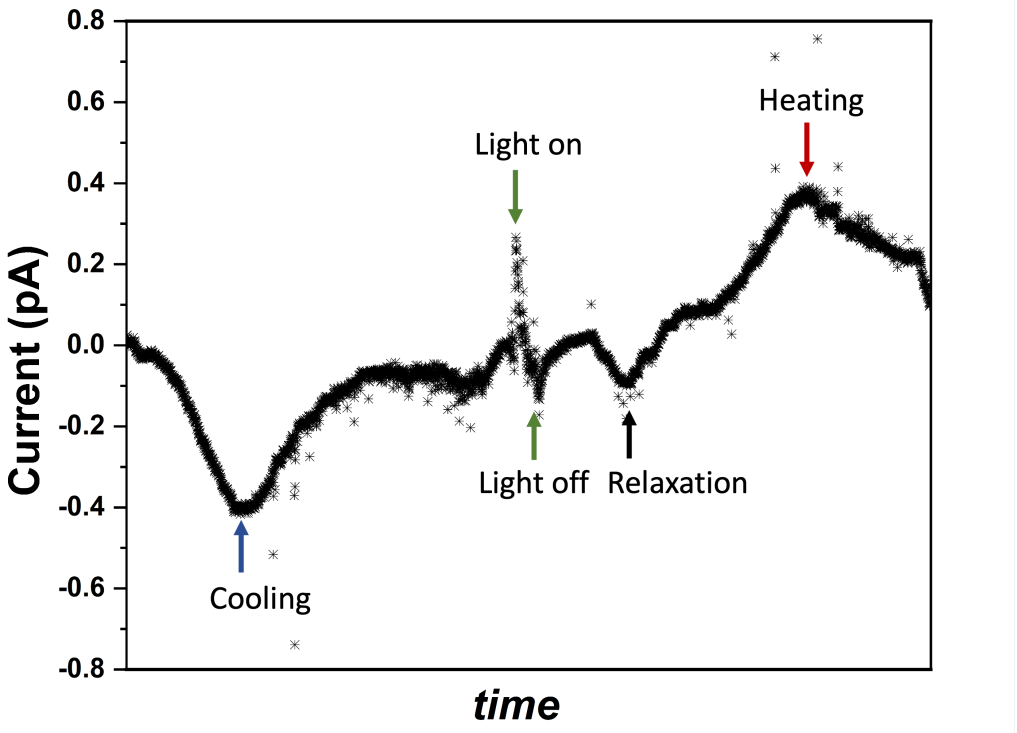

Figure S12. Light-induced pyroelectric current of compound **1·sol** before and after 532 nm light irradiation.

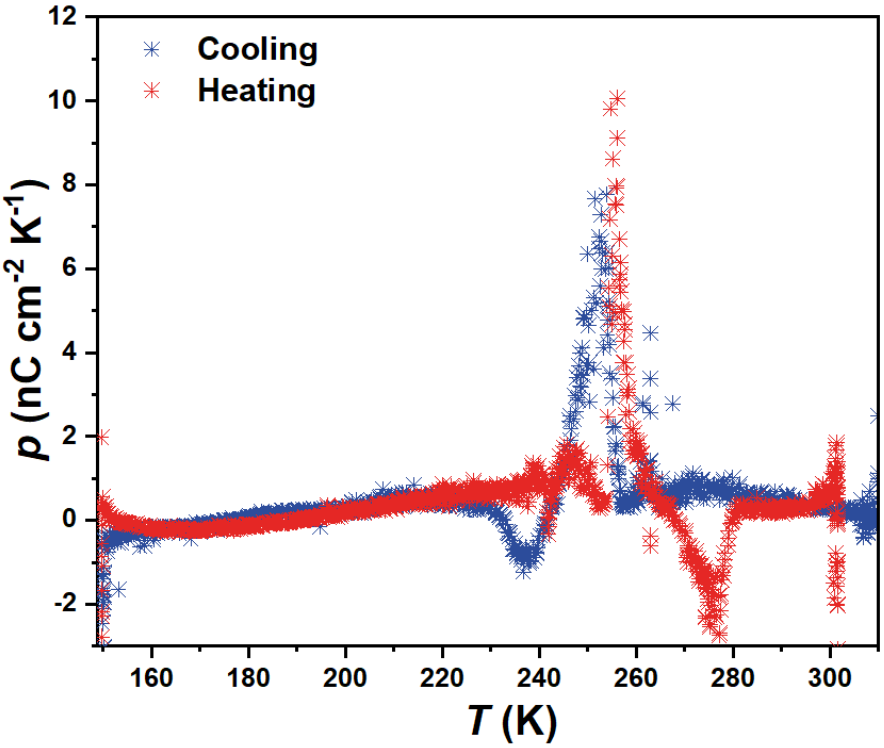

Figure S13. The pyroelectric coefficiency of compound **1**. The single crystal used for pyroelectric measurement was heated up to 310 K in the SQUID chamber for 1 h followed by a purge to remove the solvent. The desolvated sample was measured with a cycle of 310-149-300 K following the sweeping rate of 5 K min^{-1}. Even if it is difficult to obtain the accurate value of polarization change due to cracked crystal for each heating process, it still exhibited a temperature shift towards high temperature compared to that of the undesolvated form.

Table S2. Crystallographic Data Collection and Structural Refinement Information for **1·sol** and **1**.

	1·sol		**1**		
Empirical formula	$C_{38.5}H_{81}CoCrF_{18}N_8O_7P_3$		$C_{38}H_{74}CoCrF_{18}N_8O_4P_3$		
Formula weight	1313.97		1252.89		
Temperature(K)	100	200	100	150	375
Crystal system	*monoclinic*	*monoclinic*	*monoclinic*	*monoclinic*	*monoclinic*
Lattice Type	Primitive	Primitive	Primitive	Primitive	Primitive
Space group	$P2_1$(#4)	$P2_1$(#4)	$P2_1$(#4)	$P2_1$(#4)	$P2_1$(#4)
a(Å)	9.3263(2)	9.3993(2)	9.2692(2)	9.3298(2)	9.5220(5)
b(Å)	18.9286(6)	18.9744(4)	17.3930(4)	17.4539(5)	17.7433(12)
c(Å)	15.9910(4)	16.0926(3)	16.2840(4)	16.2978(4)	16.6216(9)
α(deg.)	90	90	90	90	90
β(deg.)	89.843(3)	90.051(2)	95.892(2)	95.894(3)	95.488(5)
γ(deg.)	90	90	90	90	90
V(Å^3)	2822.93(14)	2870.(05)(10)	2611.43(11)	2639.93(12)	2795.4(3)
Z value	2	2	2	2	2
D_{calc}(g/cm^3)	1.545	1.516	1.593	1.576	1.489
Light source	MoKα (λ = 0.71073 Å)				
R_1(I>2.00s(I))	0.0560	0.0480	0.048	0.0524	0.0928
wR_2(*all*)	0.1453	0.1280	0.1118	0.1252	0.2137
GOF	1.063	1.004	1.042	1.037	0.991
Flack parame-ter	0.01(2)	0.038(10)	0.033(12)	0.036(14)	0.02(2)
CCDC	2320504	2320506	2320375	2320376	2320374

[a] $\boldsymbol{R}_1 = \Sigma||F_o| - |F_c||/\Sigma|F_o|$. [b] $\boldsymbol{wR}_2 = [\Sigma\{\boldsymbol{w}(\boldsymbol{F}_o^2 - \boldsymbol{F}_c^2)^2/\Sigma\{\boldsymbol{w}(F_o^2)\}^2]^{1/2}$

Table S3. Selective bond lengths for **1·sol** and **1**.

	1·sol		**1**		
	100 K	200 K	100 K	150 K	375 K
Co-O1 (Å)	2.057	2.067	1.902	1.911	2.053
Co-O2 (Å)	2.081	2.074	1.917	1.917	2.064
Co-N1 (Å)	2.201	2.198	2.068	2.065	2.177
Co-N2 (Å)	2.111	2.112	2.027	2.028	2.110
Co-N3 (Å)	2.099	2.101	2.013	2.013	2.097
Co-N4 (Å)	2.184	2.172	2.054	2.071	2.158
Cr-O1 (Å)	1.941	1.973	1.930	1.934	2.005
Cr-O2 (Å)	1.938	1.982	1.915	1.917	2.023
Cr-N1 (Å)	2.107	2.126	2.076	2.091	2.125
Cr-N2 (Å)	2.077	2.095	2.071	2.072	2.076
Cr-N3 (Å)	2.068	2.088	2.088	2.079	2.087
Cr-N4 (Å)	2.093	2.130	2.070	2.075	2.140

Note: The structure of [CrCo] in the septet state was computationally optimized, elucidating its electronic structures and relative energies. The [CrCo] dinuclear complex was analyzed in both the high-temperature (HT) phase, corresponding to a ferromagnetic (FM) septet state, and the low-temperature (LT) phase, characterized by an antiferromagnetic (AFM) triplet state. These calculations were performed using the B3LYP*/6-311+G** level of theory.

REFERENCE

1. Tait, A. M.; Busch, D. H.; Curtis, N. F., 5,5,7,12,12,14−Hexamethyl−1,4,8,11−Tetraazacyclo−Tetradecane (5,5,7,12,12,14−Me6 [14] Ane−1,4,8,11−N4) Complexes. In *Inorganic Syntheses*, 1978, pp 10−17.

2. House, D. A.; Hay, R. W.; Akbar Ali, M. *Inorganica Chimica Acta* **1983**, *72*, 239–245.

3. S. Kanegawa, Y. Shiota, S. Kang, K. Takahashi, H. Okajima, A. Sakamoto, T. Iwata, H. Kandori, K. Yoshizawa and O. Sato, *Journal of* the American Chemical Society, 2016, 138, 14170-14173.

4. Sheldrick, G., Crystal structure refinement with SHELXL. *Acta Crystallogr. C Struct. Chem*. **71**, 3 (2015).

5. Dolomanov, O. V.; Bourhis, L. J.; Gildea, R. J.; Howard, J. A. K.; Puschmann, H., OLEX2: a complete structure solution, refinement and analysis program. *J. Appl. Crystallogr*. **42**, 339 (2009).

6. P. Sadhukhan, S.-Q. Wu, J. I. Long, T. Nakanishi, S. Kanegawa, K. Gao, K. Yamamoto, H. Okajima, A. Sakamoto, M. L. Baker, T. Kroll, D. Sokaras, A. Okazawa, N. Kojima, Y. Shiota, K. Yoshizawa and O. Sato, Manipulating electron redistribution to achieve electronic pyroelectricity in molecular [FeCo] crystals, *Nature Communications*, 2021, **12**, 4836.

7. S.-Q. Wu, M. Liu, K. Gao, S. Kanegawa, Y. Horie, G. Aoyama, H. Okajima, A. Sakamoto, M. L. Baker, M. S. Huzan, P. Bencok, T. Abe, Y. Shiota, K. Yoshizawa, W. Xu, H.-Z. Kou and O. Sato, Macroscopic Polarization Change via Electron Transfer in a Valence Tautomeric Cobalt Complex, *Nature Communications*, 2020, **11**, 1992.

8. P. Sadhukhan, S.-Q. Wu, S. Kanegawa, S.-Q. Su, X. Zhang, T. Nakanishi, J. I. Long, K. Gao, R. Shimada, H. Okajima, A. Sakamoto, J. G. Chiappella, M. S. Huzan, T. Kroll, D. Sokaras, M. L. Baker and O. Sato, Energy conversion and storage via photoinduced polarization change in non-ferroelectric molecular [CoGa] crystals, *Nature Communications*, 2023, 14, 3394.